Frequency effect on streaming phenomenon induced by Rayleigh surface acoustic wave in microdroplets

Frequency effect on streaming phenomenon induced by Rayleigh surface acoustic wave in microdroplets

M. Alghane, Y. Q. Fu, B. X. Chen, Y. Li, M. P. Y. Desmulliez, and A. J. Walton

Citation: Journal of Applied Physics **112**, 084902 (2012); doi: 10.1063/1.4758282
View online: http://dx.doi.org/10.1063/1.4758282
View Table of Contents: http://scitation.aip.org/content/aip/journal/jap/112/8?ver=pdfcov
Published by the AIP Publishing

Frequency effect on streaming phenomenon induced by Rayleigh surface acoustic wave in microdroplets

M. Alghane,[1,2] Y. Q. Fu,[1,3,a)] B. X. Chen,[1,a)] Y. Li,[4] M. P. Y. Desmulliez,[1] and A. J. Walton[4]
[1]*School of Engineering and Physical Sciences, Heriot-Watt University, Edinburgh EH14 4AS, United Kingdom*
[2]*Mechanical Engineering Department, Engineering College, University of Omar Al-Mukhtar, Al Bayda, Libya*
[3]*Thin Film Centre, Scottish Universities Physics Alliance (SUPA), University of West of Scotland, Paisley, PA1 2BE, Scotland*
[4]*Institute of Integrated Systems, Scottish Microelectronic Centre, Institute for Integrated Micro and Nano Systems, School of Engineering, University of Edinburgh, Edinburgh EH9 3JF, United Kingdom*

(Received 16 June 2012; accepted 12 September 2012; published online 17 October 2012)

Acoustic streaming of ink particles inside a water microdroplet generated by a surface acoustic wave (SAW) has been studied numerically using a finite volume numerical method and these results have been verified using experimental measurements. Effects of SAW excitation frequency, droplet volume, and radio-frequency (RF) power are investigated, and it has been shown that SAW excitation frequency influences the SAW attenuation length, l_{SAW}, and hence the acoustic energy absorbed by liquid. It has also been observed that an increase of excitation frequency generally enhances the SAW streaming behavior. However, when the frequency exceeds a critical value that depends on the RF power applied to the SAW device, weaker acoustic streaming is observed resulting in less effective acoustic mixing inside the droplet. This critical value is characterised by a dimensionless ratio of droplet radius to SAW attenuation length, i.e., R_d/l_{SAW}. With a mean value of $R_d/l_{SAW} \approx 1$, a fast and efficient mixing can be induced, even at the lowest RF power of 0.05 mW studied in this paper. On the other hand, for the R_d/l_{SAW} ratios much larger than $\sim$1, significant decreases in streaming velocities were observed, resulting in a transition from regular (strong) to irregular (weak) mixing/flow. This is attributed to an increased absorption rate of acoustic wave energy that leaks into the liquid, resulting in a reduction of the acoustic energy radiated away from the SAW interaction region towards the droplet free surface. It has been demonstrated in this study that a fast and efficient mixing process with a smaller RF power could be achieved if the ratio of $R_d/l_{SAW} \leq 1$ in the SAW-droplet based microfluidics. © *2012 American Institute of Physics*. [http://dx.doi.org/10.1063/1.4758282]

I. INTRODUCTION

Recently, there has been much interest in surface acoustic wave (SAW) technology for miniaturized microfluidic and lab-on-chip applications.[1] This technology consists of a set of interdigitated transducer (IDT) electrodes on the surface of a piezoelectric substrate as shown in Fig. 1. Surface acoustic waves can be launched by applying an alternating electric field to the IDT. When liquid (either in bulk or droplet form) lies in the propagation path of the SAW emitted by the IDT, it attenuates and changes its mode to a leaky surface acoustic wave (LSAW) upon its arrival at the boundary between solid (substrate) and liquid, due to acoustic velocity mismatch between the solid and the liquid medium.[2] This leakage of the SAW inside the droplet leads to the generation of a longitudinal pressure waves that propagates at a Rayleigh angle into the fluid,[3] as shown in Fig. 1. The absorption coefficient per unit length scale of the Rayleigh wave due to emission of longitudinal waves can be estimated using[2,4,5]

$$\alpha_l = \frac{1}{l_{SAW}} = \frac{\rho_f c_f}{\rho c \lambda}, \quad (1)$$

where ρ and ρ_f represents the densities of the $LiNbO_3$ substrate and the fluid, respectively, c_f the velocity of longitudinal wave in the fluid, c the SAW velocity in the substrate, λ is the SAW wavelength, and l_{SAW} is the attenuation length of the Rayleigh wave. The leaking of acoustic energy into the fluid medium results in a net body force, F, that generates a bulk liquid circulation within the droplet, which is known as acoustic streaming,[6,7] in a similar manner to that presented in Fig. 1.

The SAW streaming phenomenon inside microdroplets or microchannels has been previously demonstrated as an efficient technique for many microfluidic functions, such as microdroplet mixing, stirring, pumping, ejection, and atomization.[8–11] For digital microfluidics, Strobl *et al.*[12] have shown experimentally that fluorescence dye particles dissolved in water microdroplets mixed efficiently under a SAW excitation, and they reported that the duration time of the mixing process strongly depended on the radio-frequency (RF) power applied to the SAW device. Wixforth *et al.*[13,14] also have observed a similar phenomenon, where a dried fluorescent dye deposited underneath a 50 nl water droplet was dissolved and rapidly mixed with the whole droplet volume under SAW excitation. Shilton *et al.*[15] conducted an experimental study investigating the effect of IDT design on the mixing performance of SAW-driven digital microdroplets.

a)Authors to whom correspondence should be addressed. Electronic addresses: Richard.Fu@uws.ac.uk and B.Chen@hw.ac.uk.

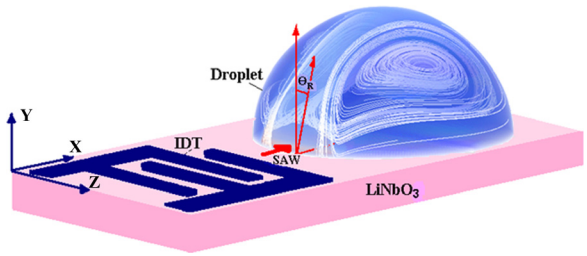

FIG. 1. Schematic illustration of SAW propagation from an IDT into a droplet showing the induced streaming patterns.

He demonstrated that the highest mixing efficiency in microdroplets was generated with transducers designed to focus the radiated SAW. Compared with the conventional IDT design shown in Fig. 1, which launches a plane wave, the focusing of the radiated SAW from the curved IDT enhances the acoustic streaming in the microdroplet. An experimental investigation by Rathgeber *et al.*[16] demonstrated that an effective mixing of liquid volumes contained in micro wells could be achieved within a couple of seconds by using SAW. For microchannel flow, Sritharan *et al.*[17] reported that, when a SAW device was placed under the junction of a Y-shaped microchannel into which two different liquids were injected, an effective mixing of the two liquids was observed under various applied powers with SAW propagating in the same direction of fluids flow in channel. Tseng *et al.*[18] investigated the effects of IDT placement (compared to SAW propagation direction) within a channel on the mixing efficiency using a parallel and transversal orientation within a Y-shaped microchannel. Results revealed that the acoustic streaming of a SAW device located in parallel within the channel performed better mixing performance than the transversal orientation, depending on the RF power applied to the SAW device.[18]

Although it is well known that the leakage of acoustic energy into the fluid medium is responsible for the SAW streaming phenomena, and the wavelength of the Rayleigh wave λ (as a part of the absorption coefficient, α_l) determines the portion of acoustic energy absorbed by the fluid, few studies have been conducted concerning the effects of wavelength (or excitation frequency) on SAW acoustic streaming.[19] For example, Tan *et al.*[20–22] reported that when the width of a grooved microchannel fabricated on the substrate surface was increased beyond an acoustic wavelength, the induced fluid flow in the microchannel by SAW excitation changed from an axially symmetric laminar flow to a vortical mixing flow, and became more chaotic with further increase in the channel width. However, there was no report on a systematic study of its mixing efficiency. Maezawa *et al.*[23] reported that modulation of the frequencies of SAW device improved mixing efficiency of liquids contained inside a liquid cell driven by a SAW, but there was no discussion of the effect of cell volume on the mixing performance. Strobl *et al.*[12] studied SAW-driven flow inside microdroplets, and experimental observations showed that a laminar flow within 5 μl droplet was disturbed by switching the device frequency between 114 and 340 MHz, which resulted in an efficient mixing for dye particles placed in water droplet.

Clearly, apart from applied SAW power that plays an important role in SAW induced mixing, the excitation frequency applied to the SAW devices represents another key parameter for enhancing the streaming phenomenon and mixing performance. Nevertheless, current literature does not provide sufficient information to quantitatively describe the influence of excitation frequency on the efficiency of mixing in SAW-based microdroplet systems. This paper investigates the effects of different flow parameters, including SAW excitation frequency, droplet volume, and applied power, using a 3D systematic simulation with experimental verification. The results provide a good guidance for the selection of optimum excitation frequency for an effective mixing device, with a minimized applied SAW power for reducing acoustic heating.

II. NUMERICAL ANALYSIS

A. Computational experiment setup

For the simulations, water droplets with volumes of 2.5, 5.0, 7.5, and 10 μl, were positioned on the SAW propagation path, as schematically illustrated in Fig. 1 and excited using 128° YX-$LiNbO_3$ SAW devices with an IDT aperture of 500 μm. Given an uniform finger spacing and SAW width,[24,25] the resonant frequency for each design IDT layout can be calculated by $f = c/\lambda = c/4d$, where c =3992 m/s,[26] where d is the IDT finger spacing or width. In this study, wavelengths ranging from 32 to 1061 μm were used.

B. Streaming model

In order to simulate the internal fluid flow of acoustic streaming for SAW-droplet coupling, the continuity equation (2) and Navier-Stoke's equation (momentum equation) (3) were used for the laminar incompressible flow driven by an external SAW body force. The verification and preliminary results of this model have been reported previously.[27,28]

$$\nabla \cdot \vec{U} = 0, \tag{2}$$

$$\frac{\partial \vec{U}}{\partial t} + (\vec{U} \cdot \nabla)\vec{U} = \vec{F} - \nabla P + v\nabla^2 \vec{U}, \tag{3}$$

where, U represents the acoustic streaming velocity, P the kinematic pressure, and v is the kinematic viscosity. F is the acoustic body force per unit mass due to the SAW-liquid interaction, which is written as; $F = -(1+\alpha_i^2)^{\frac{3}{2}} A^2 \omega^2 k_i \exp 2(k_i x + \alpha_i k_i y)$,[29] where k_i is the wave number, α_i the damping factor, ω is angular frequency, and A is the SAW amplitude which can be described using $\frac{A}{\lambda} = 8.15 \times 10^{-6} {P_D}^{0.225} + 5 \times 10^{-6} {P_D}^{0.8}$.[30] P_D is the RF power applied to the SAW device in Watts.

C. Mixing model

In order to evaluate the mixing performance of SAW-induced streaming in microdroplets, the conservation equation of mixing species was used;[31]

$$\frac{\partial m}{\partial t} + \vec{U}\cdot\nabla m = D\nabla^2 m, \tag{4}$$

where m denotes the mass fraction of mixing species (such as dye particles in this study), which is defined as the ratio of the mass of the mixing species in a given volume to the total mass of the mixture contained in the same volume. The diffusion coefficient D (diffusivity of dye in water in our case) was assumed to be 1×10^{-20} m^2 s^{-1}, and the viscosity of the dye/water solution was estimated the same as that of pure water.[32] Thus, the mass fraction function (or colour indicator) can be given as

$$m = (\text{Volume occupied by dye species})/(\text{total volume of the mixture}). \tag{5}$$

The values of the mass fraction m in Eq. (5) should be $0 \le m \le 1$, where zero corresponds to water with no dye, and a value of 1 corresponds to a volume that consists only of the dye species. Any values between 0 and 1 represent a mixture of water and dye species. By calculating the distributed values of the mass fraction, m, inside the droplet, it is possible to evaluate the mixing performance of SAW-driven microdrops.

D. Boundary conditions and solution

In this study, the maximum RF power applied to the SAW device was limited to 0.5 mW, a value which is large enough to induce efficient acoustic streaming, but without any induced droplets deformation or pumping.[27,28] In this case, the water droplet can be considered as a hemispherical body, as depicted in Fig. 2. The droplet domain was constructed using a curvilinear mesh with a grid resolution depending on the SAW wavelength, to ensure the capture of any high energy dissipation.[2] For the flow model, a non-slip boundary condition was assumed at the droplet/substrate interface, while a stress free boundary condition was applied at the interface of droplet and air. For the mixing model, zero gradient mass fractions were assumed at all the droplet boundaries. In order to visualize the whole mixing process inside the microdroplets and to evaluate the mixing performance of the SAW devices for different design parameters, the water droplets were initially (at time $t = 0$ s) assumed to have dissolvable dye particles on the droplet base with a 70 μm height from its base and with a mass fraction of $m = 1$ (the red colour base as shown in Fig. 2). In this study, an open source CFD based code OpenFOAM-1.6 (OpenCFD Ltd) was used for 3D simulations, which is based on the finite volume numerical method.[31]

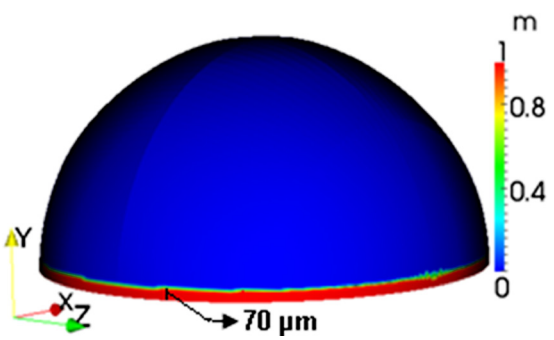

FIG. 2. Illustration showing the initial mass fraction used in this study with a value of $m = 1.0$ (dyed water) at the droplet base for a 70 μm height from its base in Y direction, and value of 0.0 elsewhere (pure water).

E. Mixing index

In order to quantify the mixing performance of such dye within the water droplet under the excitation of SAW, a mixing index parameter (*MIP*) has been used, which can be determined from the analysis of mass fraction intensity extracted from the simulation results

$$MIP = \frac{\sum_{i=1}^{N} V_i m_i}{V_0 m_{max}}, \tag{6}$$

where, N is the total number of computation cells in the droplet mesh, V_i is the localized cell volume, V_0 is the total droplet volume initially occupied by the dye species ($m = 1.0$), as shown in Fig. 2, and m_{max} is the maximum initial mass fraction of dye species (set to 1 in this study). Here, the value of *MIP* varies between 0 (unmixed) and 1 (complete mixed). Equation (6) represents the percentage of the initial dye particles at the bottom of the droplet (seen in Fig. 2) that have been propelled by the internal acoustic streaming into the pure water, or driven away from the bottom of the droplet after a SAW excitation. Thus, the defined mixing index parameter, *MIP*, can be used as a measure for describing mixing efficiency across the different simulated regimes.

III. EXPERIMENTAL

For experimental verification, the SAW devices were fabricated on 128° YX-black $LiNbO_3$ substrates by sputtering 200 nm thick aluminium to form the IDTs, with an IDT aperture of 500 μm. The details of the SAW device fabrication have been documented elsewhere.[33] The surface of the $LiNbO_3$ wafers is hydrophilic with a water contact angle of about 35° as can be observed. In this study, a spin-coated CYTOP® (Asahi Glass Co., Ltd., Tokyo Japan) layer was prepared to make the surface hydrophobic and increase the contact angle from about 35° to 110°. To agitate the liquid droplets, the SAW was generated on the surface by applying an RF signal to the IDTs using a standard signal generator MI 2019 A amplified by an MI TF2175 RF power amplifier. Water droplets with volumes ranging from 2.5 to 10 μl were loaded at the centre of the SAW propagation path by using a micro-volume kit micropipette, as shown in Fig. 1. In addition to droplet volume and SAW wavelength, the effect of a moderate range of applied RF powers from 0.05 to 0.5 mW were evaluated. These were selected to ensure that the droplet would not be dramatically deformed but sufficient energy would be available to induce internal streaming and mixing inside the droplets. In order to determine the streaming velocity, polystyrene particles with average diameters of 6 μm were placed inside the water droplets and their motion was recorded using a high speed camera (Kodak Motion Corder Analyzer—600 frames per second). In order to experimentally visualize the whole mixing process inside the

microdroplets and to evaluate the mixing performance of the SAW devices for different design parameters, dried particles of food dye were initially placed underneath the droplets (at time $t = 0$ s), and their mixing process inside the droplets after the SAW power was tracked.

IV. COMPARISON AND DISCUSSION

A. Acoustic mixing process

The characteristic mixing process of SAW-induced microdroplets mixing will be discussed first. Figure 3 presents sequential images of the simulated mixing process of the dye in a 5 μl droplet. Here, an RF power of 0.5 mW was applied to the SAW device, and an excitation frequency of $f = 39.92$ MHz (corresponding wavelength, $\lambda = 100\ \mu$m) was used. First column (a) in Fig. 3 shows 3D volume images of the changes of dye concentration with the time period after the SAW excitation. After applying an RF power to the IDTs of the SAW device, a SAW was launched and coupled with the water droplet. Its energy is radiated into the droplet at a Rayleigh angle, inducing an effective acoustic momentum (body force) that decays exponentially away from the SAW interaction region. This momentum source at the SAW-droplet interaction region establishes a flow field that drives the fluid upwards at a Rayleigh angle, resulting in build-up of a progressive flow within the droplet, as seen in the left hand column of Fig. 3 after 0.03 s. It can be observed that in Fig. 3 (column (a)), the streaming velocities are the highest near the SAW source, especially during the early stages of flow development.

Simultaneously, the generated flow in the droplet induces an advection for the dye particles at the bottom of the droplet towards the top of the droplet at the same Rayleigh angle of longitudinal pressure wave. This is clearly observed in the early stage images presented in column (a) of Fig. 3. The flow is guided by the curved droplet/air interface back down towards the droplet base where it is then directed back towards the SAW excitation source along the base of the droplet. When this reverse flow reaches the region near the SAW source, the SAW drives the reverse flow upwards again, causing an advection for more dye particles that travels away from the droplet bottom into the droplet volume. Finally, after a few seconds, the developed flow reaches a steady stage of the double vortex (butterfly) flow patterns,[34] as shown by the velocity vectors in the latest stages of column (a) (time = 7 s) in Fig. 3. This steady flow pattern is dependent on the excitation frequency, the applied SAW power, the droplet size, and the fluid properties.[27,28,35]

For further analysis, the mass fraction data were divided into two groups; with the first group covering the mass fraction range of 0-0.5 and the second one from 0.5 to 1.0. The second column (b) in Fig. 3 shows the simulated contours of mass fraction ranging from 0 to 0.5 using 3D clips (e.g., 3D droplet volume images with cutting planes along the Y and Z axis showing half of hemispherical body). These results show that the dye particles follow the fluid flow in similar patterns with an increasing dye mixing volume inside the whole droplet. The dye mixing volume increases continually as the dye is fed from the dye particles at the droplet bottom, through streaming-induced advection. This advection of the dye particles results in a decrease in the volume of the high concentration zone ($m \geq 0.5$) with the development of streaming flow, as shown in the third column (c) of Fig. 3 that covers a higher mass fraction range of 0.5-1.0. Also, it can be observed from Fig. 3(c) that the quantity of dye particles driven from the droplet base decreases with the duration of streaming flow. Eventually, the concentration of the dye particles that dissolved in the water droplet reaches a steady state value and the solution nearly becomes homogeneous.

Figure 4 shows that the simulation results are identical to our experimental observations as well as those from literature.[12,36] For comparison, dried particles of food dye were deposited underneath a 5 μl water droplet before applying the RF power. Figure 4 depicts four snapshots of such mixing experiments of SAW-induced streaming. After applying the RF power, the dye is quickly mixed in the droplet in a few seconds. As can be observed from the snapshots of the dye mixing in droplet, the coupled SAW from the bottom of the droplet induces an acoustic streaming that leads to an advection for the food dye particles at the bottom of the droplet (in blue colour) towards the top of the droplet at the Rayleigh angle of longitudinal pressure wave, as indicated by the black dashed arrow in Fig. 4 at time of 1 s, which agrees well with the results presented in Fig. 3 at the same duration time. Finally, the dissolving process of the dye particles reaches a steady state distribution inside the droplet volume, as can been seen from both the numerical and experimental observations presented in Figs. 3 and 4, respectively, at a duration of 7 s.

B. Mixing efficiency versus SAW excitation frequency

The relation between the mixing efficiency and excitation frequency (or wavelength) was studied and the values of the *MIP* were investigated as functions of droplet volume, wavelength, and RF power. Figure 5(a) shows the derived mixing efficiency as a function of a dimensionless ratio between the droplet radius, R_d, and the estimated attenuation length of a Rayleigh wave, l_{SAW},[2] i.e., R_d/l_{SAW}. In this case, a 5 μl water droplet was used, and a 500 μm aperture SAW device was excited with an applied RF power of 0.5 mW. In order to derive more information about the effectiveness of SAW-induced convective mixing, the relationship between *MIP* and R_d/l_{SAW} was studied for different ranges of mass fraction. As can be observed in Fig. 5(a), the *MIP* profile that covers the whole range of mass fraction ($m \leq 1.0$) shows only minimal variation with R_d/l_{SAW} and gives little insight into the effectiveness of the value of R_d/l_{SAW} on the mixing efficiency of SAW devices. Comparing these results with other mass fraction ranges in Fig. 5(a), the trends for both the profiles for $m \leq 0.1$ and $m \leq 0.5$ are similar and show clearly that there is a critical value of $R_d/l_{SAW} = 0.92$, beyond which there is a considerable decrease in the mixing efficiency (e.g., reducing l_{SAW} as an increase in the excitation frequency or a decrease in wavelength). With the acoustic energy loss being the dominant mechanism for the generation of acoustic streaming, coupled with minimal acoustic

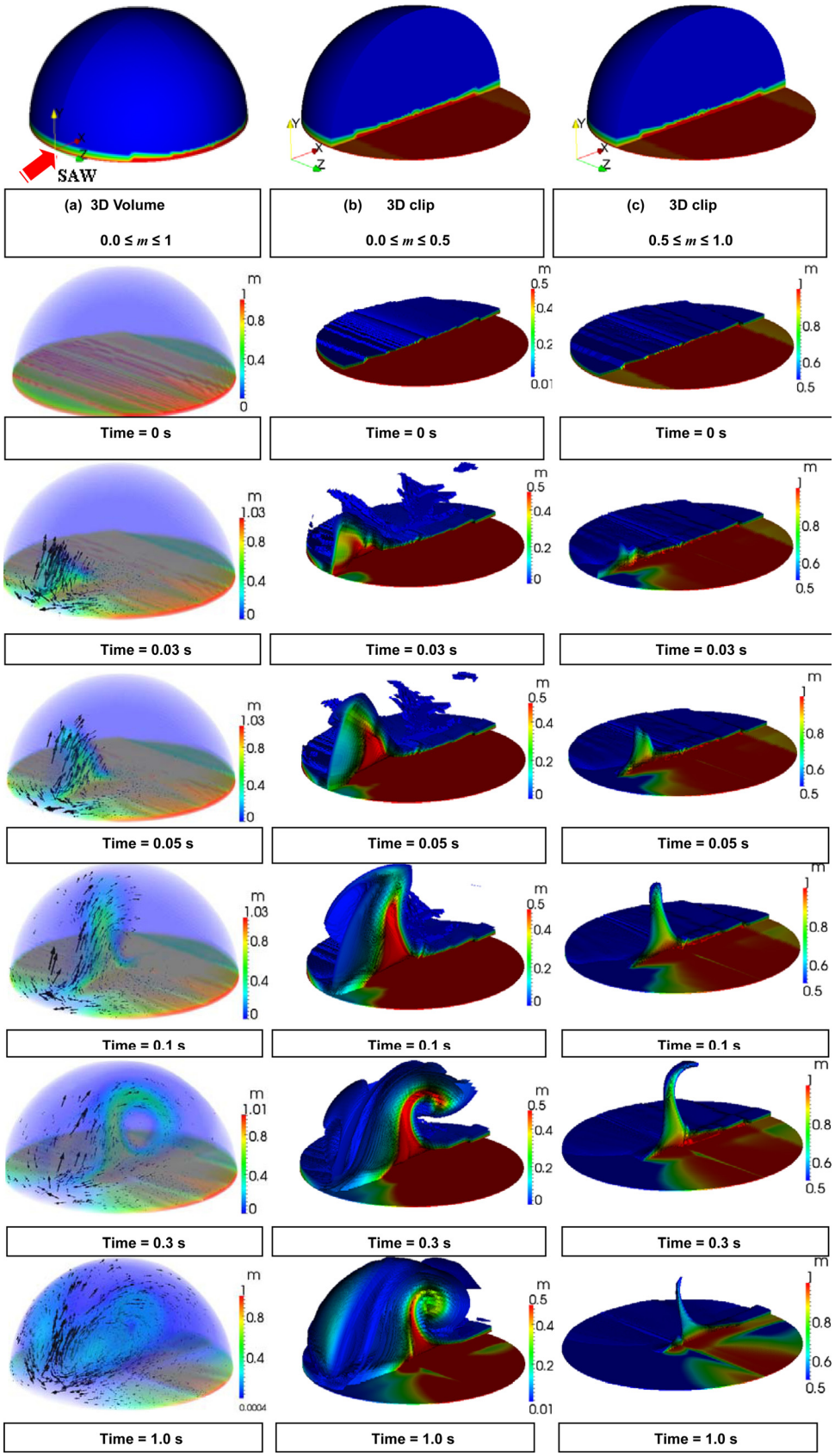

FIG. 3. Three dimensional images of the simulated mixing process for a 5 μl water droplet, using 128° YX-LiNbO3 SAW devices with 0.5 mm SAW aperture and excited by frequency of 39.92 MHz at an RF power of 0.5 mW. The first row shows different illustrations of the droplet at different views and mass fraction ranges; Column (a): the mixing process in 3D volume images using mass fraction range $0.0 \leq m \leq 1$, and the black arrows indicate to the velocity vectors of the flow field; Column (b): 3D images of the mixing process looking through the droplet that induced by cutting slices into it, as shown in the first row, using smaller range of mass fraction $0.0 \leq m \leq 0.5$; column (c) similar to column (b) but covers the largest mass fraction range of $0.5 \leq m \leq 0.1$.

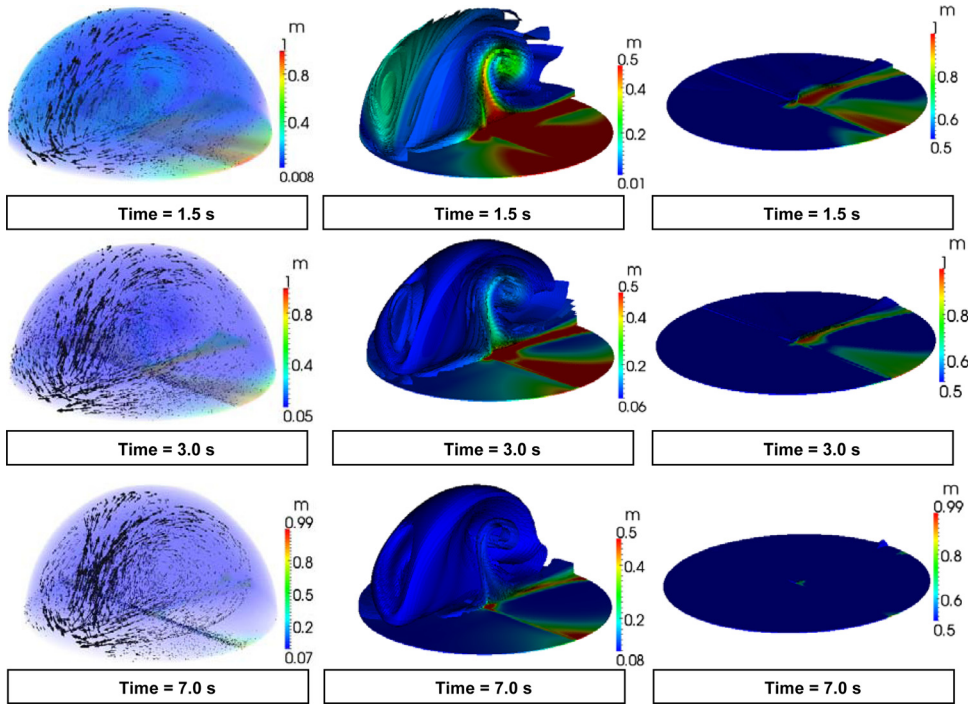

FIG. 3. *(Continued.)*

heating resulting from the low RF power and fluid viscosity,[37,38] this flow phenomenon can only be explained by the acoustic energy that is absorbed by the liquid layer. Based on the results presented in Fig. 5(a), the *MIP* profile has more sensitivity to the variation of the R_d/l_{SAW} ratio when the mass fraction of $m \leq 0.1$ (a value that corresponds to mean mass fraction, $m_{mean} = 0.1$). Hence, the mass fraction range of $m \leq m_{mean}$ was used in this study to quantify the SAW mixing efficiency, where m_{mean} is the mass fraction of homogenous mixing, which can be calculated by the ratio of initial dye volume to total droplet volume and the maximum initial mass fraction, $m_{mean} = m_{max}V_0/V_{tot}$.

Figure 5(b) presents the simulated steady state (the time after which there is no changes in the dye concentration) results of 3D clip images, showing the effect of R_d/l_{SAW} ratio on the dye homogeneity (or mixing efficiency). From the image of first column (corresponding to $R_d/l_{SAW} = 0.92$), the droplet mixture is shown to be extremely homogeneous and the dye particles are distributed uniformly across the whole droplet volume, with a mass fraction value of $m \approx 0.1$ everywhere inside the droplet. In contrast, when the R_d/l_{SAW} ratio is larger than one, such as 1.43 in Fig. 5(b)), an inhomogeneous mixture is obtained with less dye particles transported into the droplet volume, due to the weakness of acoustic streaming flow, which can be seen from the results of $m \leq 0.1$ shown in Fig. 5(a). This flow becomes much slower with further increases in the R_d/l_{SAW} ratio. For example, a value of 3.35 in Fig. 5(b) resulted in larger area of the dye

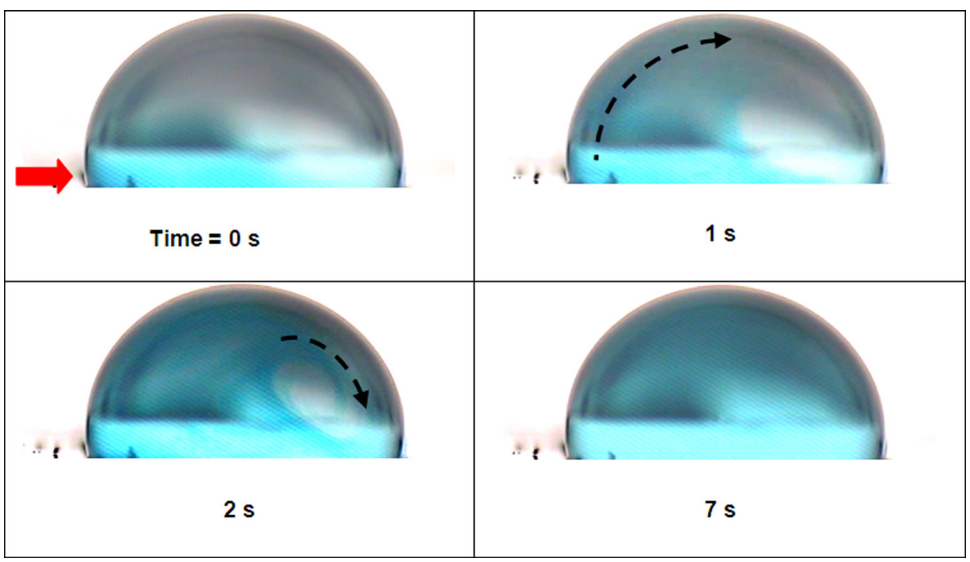

FIG. 4. Side view snapshots of SAW-induced internal streaming in a 5 μl water droplet, where dried particles of food dye were placed underneath the droplets. After the SAW excitation, the dye colour quickly fills the whole droplet volume. The black arrow with dash line shows the fluid flow inside the droplet, and the red arrow indicates to the direction of the SAW propagation.

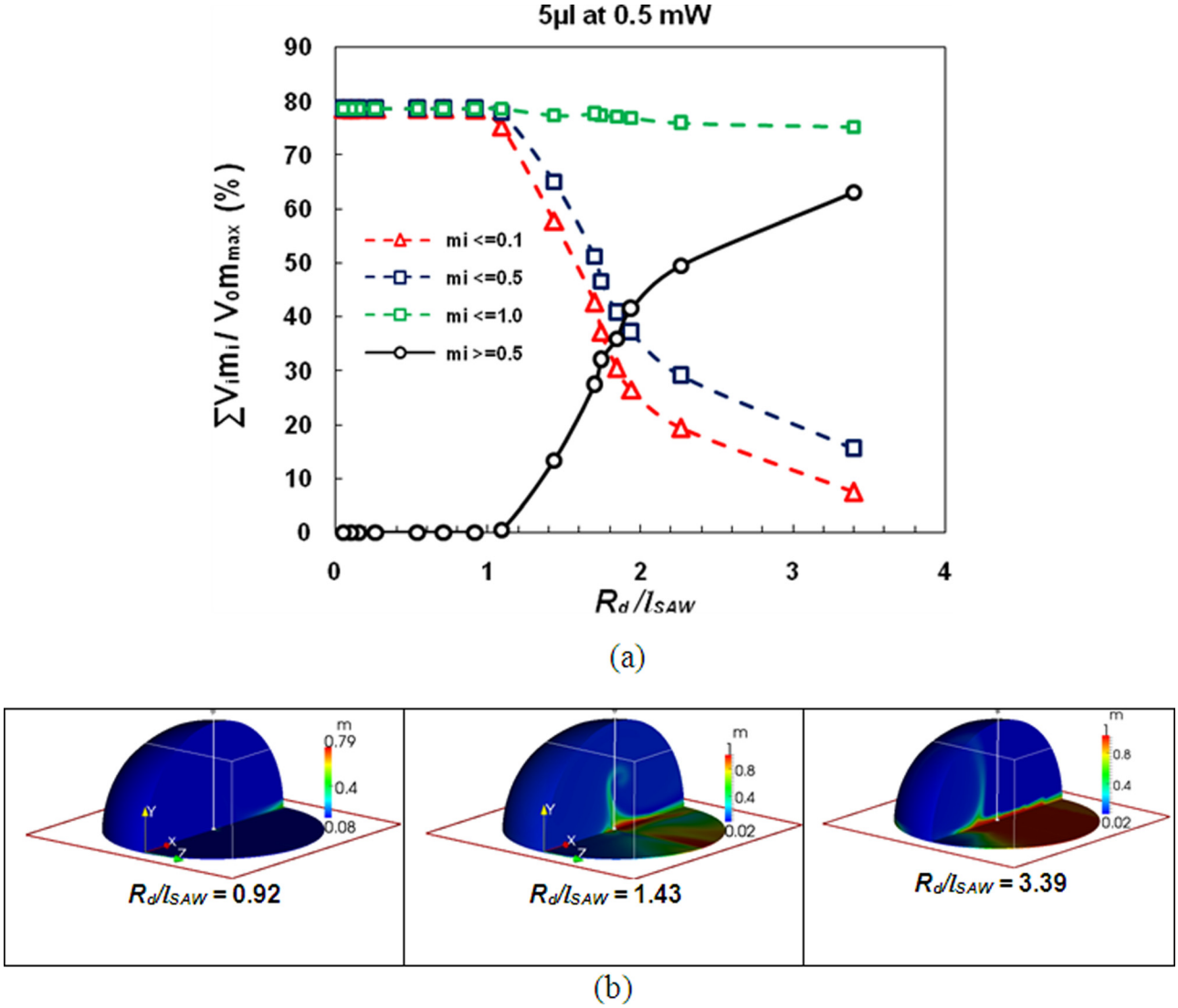

FIG. 5. Normalised mixing intensity results for a 5 μl droplet, using 500 μm aperture SAW device at a RF power of 0.5 mW, and with an initial mass dye particles concentration of $m = 1$ for a 70 μm high from the droplet base and $m = 0$ elsewhere (pure water); (a) deviation in the steady state mixing intensity as a function of R_d/l_{SAW} for different mass fraction ratios (b) 3D captured clips of the droplet showing the effect of R_d/l_{SAW} ratio on mixing efficiency.

particles that clustered at the droplet bottom, with high concentrations (e.g., $m \geq 0.5$). This can also be verified by mixing efficiency shown in Fig. 5(a) for the curve of $m \geq 0.5$. When the value of R_d/l_{SAW} exceeds a unity, the percentage of the droplet volume that contains a high concentration dye particles significantly increases and reaches up to 60% with further increases in R_d/l_{SAW}, indicated by the case of $m > 0.5$ show in Fig. 5(a). This clearly shows that the SAW mixing becomes poorer at high frequencies.

Figure 6 presents the *MIP* as a function of R_d/l_{SAW} ratio at three different RF powers (0.05, 0.15, and 0.50 mW) using a 2.5 μl droplet with an initial dye concentration similar to that shown in Fig. 2. Generally, the relationship for each power in Fig. 6 shows a similar trend to that of 5 μl droplet in Fig. 5(a) for equal mass fraction range of $m \leq 0.1$. This indicates that the mechanism of the dye mass transported by a bulk liquid circulation of SAW excitation is similar. However, beyond a critical R_d/l_{SAW} ratio which is dependent upon the RF power, further increase in this ratio results in a considerable decrease in the mixing efficiency. The results show

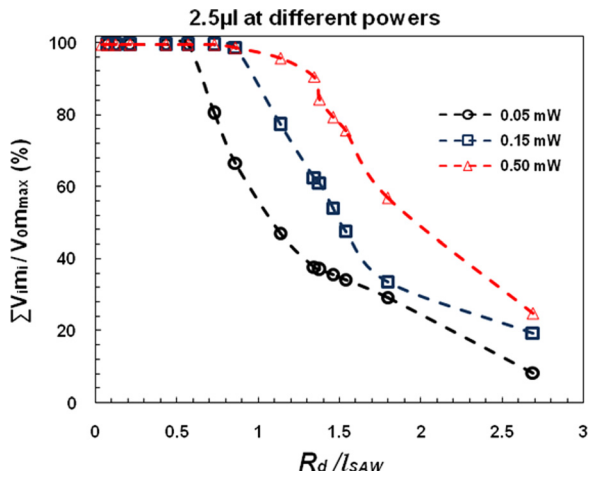

FIG. 6. Variation of mixing efficiency for 2.5 μl droplets as a function of R_d/l_{SAW} for different RF power, using 500 μm apertures SAW devices.

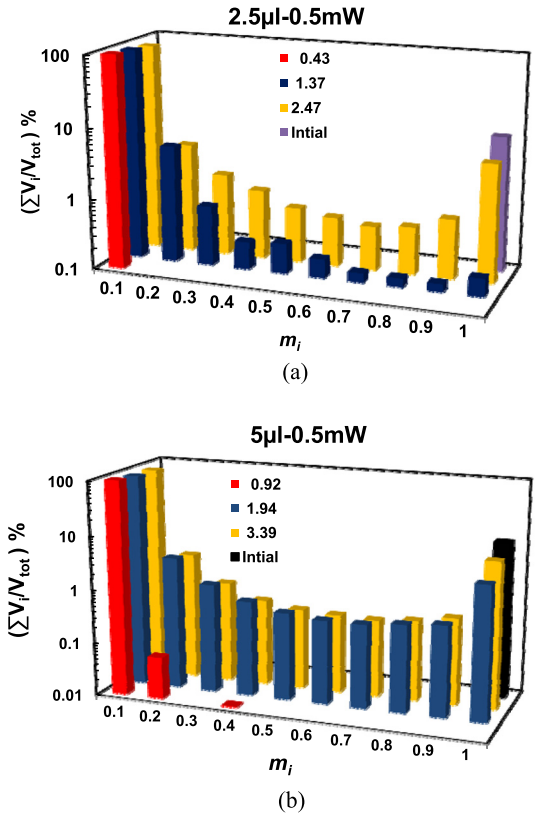

FIG. 7. PDF quantifying the distributions of the dye particles for different R_d/l_{SAW} ratios at 0.5 mW RF power; (a) for 2.5 μl droplets; (b) for 5 μl droplets. The probability values of the histogram were obtained through moralizing the total mixing volume V_i by a total droplet volume V_{tot}.

that the critical ratio of R_d/l_{SAW} decreases from 0.86 at an RF power of 0.5 mW to about 0.6, when a lower RF power of 0.05 mW is applied to the SAW device. This could be the result of less acoustic energy being absorbed by the water droplet with the same fluid inertia, causing a slow streaming flow, and thus a less mixing efficiency.[28] It is also interesting to note from the results that when the R_d/l_{SAW} ratios are much smaller than one, a mixing efficiency of 100% can be obtained even with a small value of SAW powers of 0.05 mW. This reveals that if the condition of mean critical ratio of $R_d/l_{SAW} \leq 1.0$ has been reached, the devices with a lower frequency could induce an efficient mixing, even with low SAW powers.[27]

In order to further clarify the role of the R_d/l_{SAW} ratio (e.g., acoustic wavelength or frequency) in the SAW-droplet based mixing system, a probability distribution function

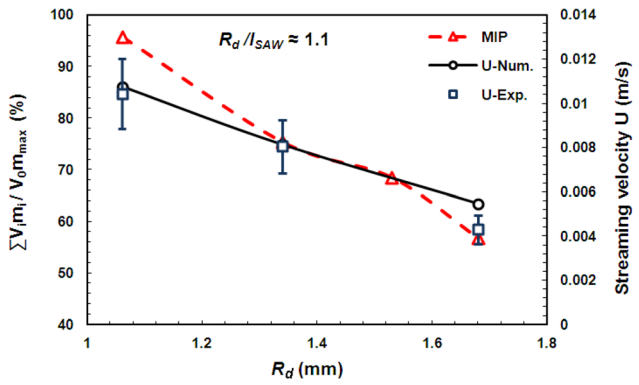

FIG. 8. Variation of mixing efficiency, and streaming velocity (both from experiment and simulation) as a function of droplets radius, using 500 μm apertures SAW devices with $R_d/l_{SAW} \approx 1.1$ and 0.5 mW RF power.

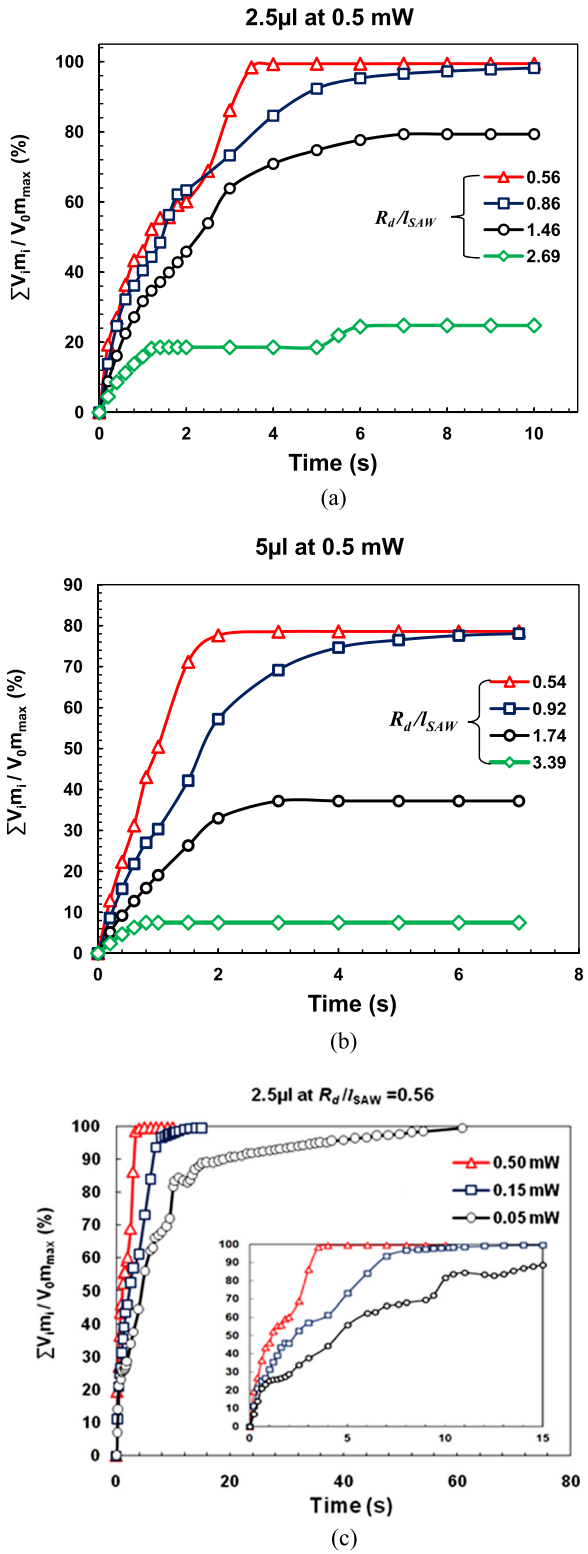

FIG. 9. Mixing efficiency (*MIP%* for m_{men}) as a function of time for (a) 2.5 μl water droplets—RF power of 0.5 mW, (b) 5 μl water droplets—RF power of 0.5 mW, (c) of 2.5 μl water droplets at $R_d/l_{SAW} = 0.56$ for different RF powers of 0.015, 0.05, and 0.5 mW.

(PDF) of the dye particles concentration, m, was calculated at three different R_d/l_{SAW} ratios for two droplets of 2.5 and 5.0 μl, and at a duration time of steady state mixing (no variation in the dye concentration in droplets with further increase in duration time). The PDFs were obtained through calculating the total mixture (e.g., dye/water) volume contained in the droplet, V_i, for a set of mass fraction groups, m_i, which were further normalized by the total volume of the droplet, V_{tot}. The mass fractions were classified into 10 groups ranging from 0 to 1.0, in order to distinguish and quantify the mixing performance for each R_d/l_{SAW} ratio, as shown in Fig. 7, using log-scale. Figure 7(a) shows that for a 2.5 μl droplet, the value of PDF initially is about 10% (with mass fraction of one). Under SAW excitation, the dye particles distribute across the volume of water droplet and reach a steady state distribution in a few seconds. However, the mixing behavior depends strongly on the value of the Rd/l_{SAW} ratio. For the ratios smaller than a mean value of 1.0, such as $R_d/l_{SAW} = 0.43$ presented in Fig. 7(a), the histogram of PDF has only one component at a mass fraction of $m_i = 0.1$, indicating a homogeneous mixture, and an effective SAW-induced mixing. In contrast, for larger R_d/l_{SAW} ratios, such as 1.37 and 2.47 presented in Fig. 7(a), non-uniform distributions of the dye particles inside the water droplet are obtained. With further increases in the R_d/l_{SAW} ratio above one, clustering of high concentration dye particles of $m \geq 0.5$ at the droplet bottom is observed, as shown in Fig. 5(b), indicating that mixing is inefficient. In general, the data in Fig. 7(b) for a 5 μl water droplet show similar behaviours to those in Fig. 7(a) where good mixing is achieved when the R_d/l_{SAW} ratios are less than 1.0.

However, results show that the SAW-induced mixing within a small droplet is more homogeneous than that of larger volumes with the same R_d/l_{SAW} ratios. Figure 8 shows the variation of the *MIP* as a function of droplet radius R_d at an RF power of 0.5 mW with an R_d/l_{SAW} ratio of ~1.1. As can be seen clearly, an increase in the droplet radius (or size) results in a decrease in the mixing efficiency. This can be explained by the increase of liquid inertia for a larger droplet, resulting in a slower streaming velocity (e.g., measured at the top centre of droplets) as shown in Fig. 8. This has been verified based on both simulations and experimental observations using a high speed camera (Kodak Motion Corder Analyzer—600 frames per second).

Effects of the R_d/l_{SAW} ratios on variations of *MIP* as a function of time were also investigated for different droplet volumes and RF powers. Figures 9(a) and 9(b) show the development of dye particles mixing inside water droplets of 2.5 and 5.0 μl volumes, respectively, with an applied SAW power of 0.5 mW. After an RF power is applied to the SAW device, a non-zero *MIP* value is obtained, which increases gradually and finally approaches a steady-state value, depending on the SAW power, excitation frequency, and droplet volume. As clearly shown in Figs. 9(a) and 9(b), the mixing rate and efficiency are determined by the value of R_d/l_{SAW} ratios (or SAW frequencies). Fast mixing processes are obtained when the R_d/l_{SAW} ratios are smaller than one. In contrast, when R_d/l_{SAW} ratios are larger than one, lower mixing rates and efficiencies are induced, as shown in Figs. 9(a) and 9(b). For instance, from data in Fig. 9(b), the values of mixing rate and mixing efficiency for the R_d/l_{SAW} ratio of 0.54 are $\sim 48\,s^{-1}$ and ~79%, respectively, whereas these are only $\sim 18\,s^{-1}$ and ~37% for an R_d/l_{SAW} ratio of 1.74. From the profiles in Figs. 9(a) and 9(b), the mixing efficiencies for the R_d/l_{SAW} ratios less than an unity are similar for the same droplet volumes and are about 100% for of 2.5 μl and 80% for of 5 μl droplet, even though the mixing rate was different for the different ratios. These results confirm that the SAW-driven convective mixing is inefficient when the $R_d/l_{SAW} \gg 1.0$.

Figure 9(c) shows the variation of the *MIP* as a function of time for three different applied RF powers of 0.05, 0.15,

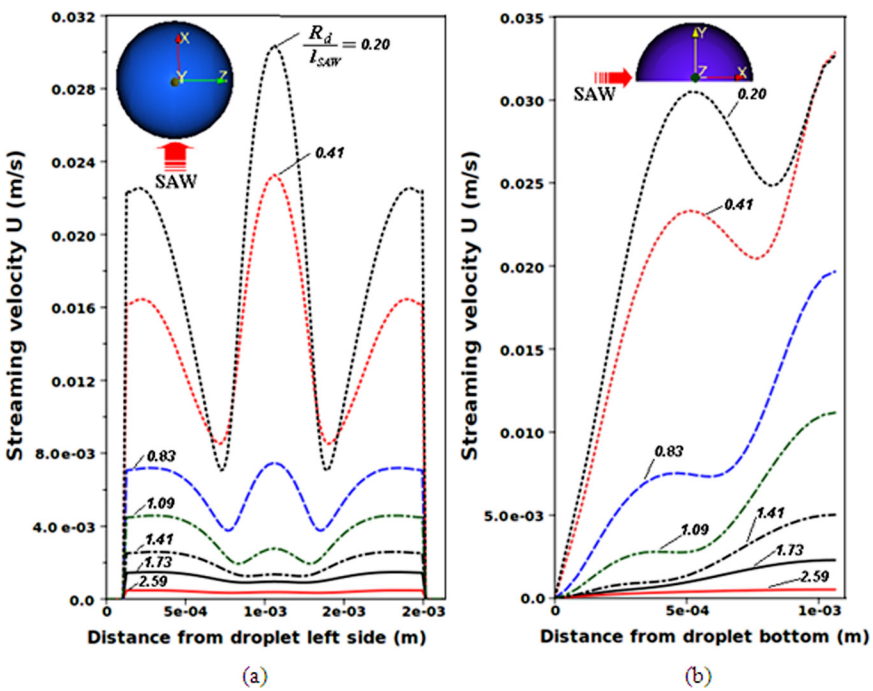

FIG. 10. Simulated streaming velocity profiles measured along two different axis into a 2.5 μl droplet for a range of R_d/l_{SAW} ratios, using 500 μm aperture SAW device with an RF power of 0.5 mWatt; (a) measured along the z axis at 500 μm height from the droplet bottom; (b) radial distribution measured along the y axis at the droplet centre.

TABLE I. Characteristic flow parameters for numerical simulation of 5.0 μl droplet at RF power 0.5 mW.

Wavelength (μm)	Excitation frequency (MHz)	R_d/l_{SAW}	SAW amplitude (A°)	Streaming force (N/kg)	Streaming velocity (m/s)	*MIP %*
200	19.96	0.543743	2.971	14.524	0.032573	78.61178
117.888	33.862	0.922474	1.752	24.641	0.021347	78.42174
100	39.92	1.087486	1.485	29.012	0.016342	75.35968
75.7857	52.6748	1.434949	1.125	38.288	0.008128	57.87846
58.944	67.7274	1.844947	0.875	49.282	0.00312	30.50193
32	124.75	3.398393	0.4755	90.778	0.00027	7.487235

and 0.5 mW for a 2.5 μl droplet with the R_d/l_{SAW} ratio fixed at 0.56. This shows that the mixing rate is enhanced and mixing time is reduced with an increase in the RF power. For example, the mixing duration is only 4 s at an RF power of 0.5 mW, while it is 61 s at 0.05 mW. Nevertheless, the steady state value of mixing efficiency is not influenced significantly by the applied RF power, whereas the results presented in Figs. 9(a) and 9(b) clearly show that the mixing efficiency changes significantly with the R_d/l_{SAW} ratio (e.g., SAW excitation frequency).

C. Acoustic streaming versus SAW wavelength

The effects of a droplet volume and applied power on the streaming flow have been reported.[28] In this section, acoustic streaming phenomena and flow patterns were investigated for different R_d/l_{SAW} ratios. Figures 10(a) and 10(b) present the distribution of simulated streaming velocities for a 2.5 μl water droplet with different R_d/l_{SAW} ratios, measured along the z and y axis of the droplet. Clearly, a decrease in the R_d/l_{SAW} ratio results in an enhancement in the streaming velocities. When the R_d/l_{SAW} ratio is less than one, higher velocity gradients are observed inside the droplet, whereas smaller gradients are seen for R_d/l_{SAW} ratios larger than one, indicating a weakness of flow circulation by SAW excitation. These results support those in Figs. 5 and 6, i.e., with the higher the velocity gradient in the droplet, the better the mixing process, due to a stronger streaming-driven convection being produced. Therefore, the larger the shear velocity gradients across the droplet axis, the faster the convective velocities that transport the dye particles into the bulk droplet, resulting in a more efficient mixing process.

To clarify the physics behind the effects of the R_d/l_{SAW} ratio, the characteristic flow parameters of a 5.0 μl droplet with an applied power of 0.5 mW were calculated, and the results are listed in Table I. This shows that although the streaming force is enhanced, the increase in the excitation frequency (or decrease in wavelength) offsets the increase of streaming velocity (measured at the top centre of droplet). These conflicting mechanisms can be attributed to the decrease in the SAW attenuation length, l_{SAW},[2,4] due to the increase in the excitation frequency, which causes the SAW acoustic energy to be strongly absorbed by the liquid, and hence the higher rate of energy dissipation. Consequently, the more rapid the acoustic energy dissipation, the smaller the energy to be reach the droplet top free surface, which in turn results in a slower flow circulation due to a large fluid inertia, and less effective mixing.

Figure 11 shows the simulated distribution profiles of SAW streaming force along the propagation path of the longitudinal wave starting from the SAW interaction point (near SAW source) towards the top centre of a 5.0 μl water droplet and for different R_d/l_{SAW} ratios, using a 500 μm aperture SAW device at an applied RF power of 0.5 mW. Fig. 11 shows that the streaming forces decrease with the distance from the interaction region of SAW, which indicates damping of the wave. Comparing results for the different R_d/l_{SAW} ratios, the value of streaming force at the interaction region (near the SAW source) is enhanced by increasing the ratio of R_d/l_{SAW}. Nevertheless, the momentum of acoustic energy (streaming force) that is transferred away from the SAW interaction region decreases significantly with an increase in the R_d/l_{SAW} ratio, especially when the R_d/l_{SAW} ratio is larger than one. This is attributed to an increase in attenuation rate with increasing the SAW excitation frequency as listed in Table I.

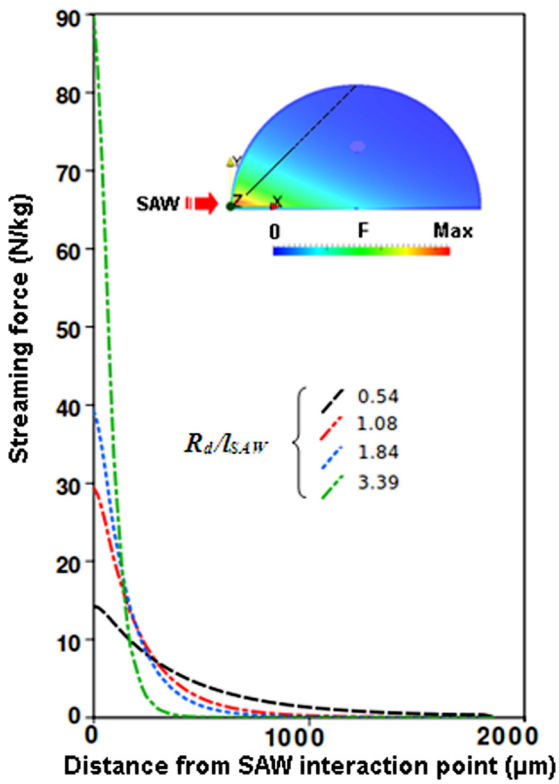

FIG. 11. Measurements of acoustic streaming force at SAW interaction point and along the propagation direction of the longitudinal wave towards the top centre of 5.0 μl droplet, and for R_d/l_{SAW} ratios; the black line into the droplet show the measuring path of acoustic streaming force.

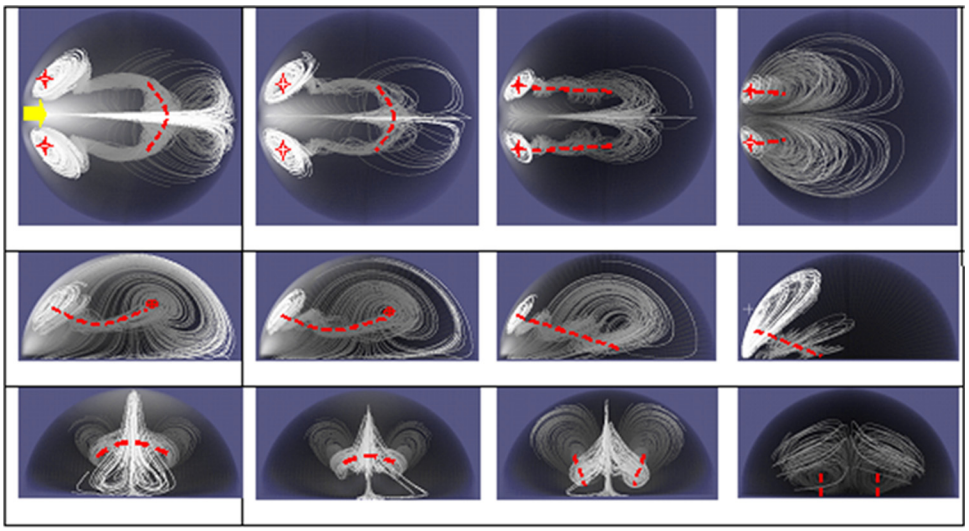

FIG. 12. Simulated results showing the changes in the streaming patterns with R_d/l_{SAW} ratio, and for 2.5 μl droplet using 0.5 mm aperture SAW device and 0.5 mW RF power. The first row shows a top view of the double vorticity; the second row shows the side view focusing through the droplet centre, and the third row views the droplet from the front. The yellow arrow indicates to the SAW direction, and the red broken lines the axis of rotation.

Figure 12 presents the simulation results of the flow streaming patterns induced by SAW excitation in a 2.5 μl droplet with an applied RF power of a 0.5 mW for a range of R_d/l_{SAW} ratios. These results show that the flow patterns are strongly affected by the frequency, especially for a high excitation frequency, or the R_d/l_{SAW} ratios larger than one. Therefore, the streaming patterns can be classified into two groups based upon the shape of the flow axis of rotation. The first group is associated with the ratio of $R_d/l_{SAW} \leq 1.0$ and the regular butterfly patterns are observed, where the fluid flow rotates about one elliptical axis of rotation through the droplet centre in a similar manner to those shown in the first and second column in Fig. 12. In the second group, when the ratio of $R_d/l_{SAW} \gg 1.0$, such as 1.41 and 2.93, an irregular (weak) streaming pattern results, where the fluid flow rotates about two individual axes of rotation, as shown in the third and forth column in Fig. 12. When the regular butterfly patterns are induced by the SAW with a ratio of $R_d/l_{SAW} \leq 1.0$, the strong interaction between the driving flow and back flow contributes to the mixing efficiency. This is confirmed by results of different mixing index parameters presented in Figs. 5 to 8, showing effective mixing and better homogeneity for the solution mixture. In contrast, an ineffective mixing were induced for an $R_d/l_{SAW} \gg 1.0$, where the longitudinal pressure wave arriving at the droplet free surface is strongly attenuated thus resulting in a weak acoustic streaming force. This demonstrates that the streaming velocity, flow profiles, and mixing efficiency all are influenced by the SAW excitation frequency.

V. CONCLUSIONS

In summary, a SAW-driven mixing process of the dye particles inside microdroplets has been simulated numerically and verified experimentally, in order to investigate the effect of SAW excitation frequency (or wavelength) in the flow streaming and mixing process for a range of droplet volumes and RF powers. It has been shown that a higher RF power and a decreased droplet size results in an increase in the streaming velocity and mixing efficiency, whereas a higher excitation frequency can result in less effective mixing with a slower mixing rate, due to weakness of streaming flow. The SAW attenuation length, l_{SAW} (a factor directly related to the SAW excitation frequency and wavelength), has been identified as a parameter indicating the efficiency of SAW-inducing convective mixing. A fast and effective mixing process results until l_{SAW} reaches a critical value, beyond which a significant decrease in streaming velocity and mixing efficiency is observed. The magnitude of streaming velocity, mixing rate, and efficiency were determined by the droplet size to be a highest when the ratio of the droplet radius to SAW attenuation length $R_d/l_{SAW} \leq 1.0$, even at small SAW powers, such as 0.05 mW. In contrast, inhomogeneous mixtures with slower mixing rates were obtained when $R_d/l_{SAW} \gg 1.0$, due to the higher attenuation rate of acoustic energy and minimization of energy reaching the droplet free surface. As a high power results in a significant heating effect, this mean critical ratio ($R_d/l_{SAW} \leq 1$) can be used as a guideline in the SAW device design for microfluidic applications that include temperature sensitive biological samples inside the microdroplet.[38,39]

ACKNOWLEDGMENTS

The authors acknowledge the support from the Innovative electronic Manufacturing Research Centre (IeMRC) through the EPSRC funded flagship project SMART MICROSYSTEMS (FS/01/02/10). Financial support from Royal Society-Research Grant (RG090609), Carnegie Trust Funding, and the Royal Society of Edinburgh is also acknowledged.

[1]A. Manz, N. Graber, and H. M. Widmer, Sens. Actuators B **1**(1-6), 244–248 (1990).
[2]R. M. Arzt, E. Salzmann, and K. Dransfeld, Appl. Phys. Lett. **10**(5), 165–167 (1967).
[3]M. K. Kurosawa, Ultrasonics **38**, 15–19 (2000).
[4]K. Dransfeld and E. Salzmann, in *Physical Acoustics*, edited by W. P. Mason and R. N. Thurston (Academic, New York, 1970), pp. 219–272.
[5]L. Schmid, A. Wixforth, D. Weitz, and T. Franke, Microfluid. Nanofluid. **12**(1), 1–7 (2011).
[6]W. L. Nyborg, in *Physical Acoustics*, edited by e. W. P Mason (Academic, 1965), pp. 265–331.
[7]W. L. Nyborg, in *Nonlinear acoustics*, edited by M. F. Hamilton (Academic, New York, 1998), pp. 207–331.

[8]N. I. Newton, M. K. Banerjee, T. K. H. Starke, S. M. Bowan, and G. McHale, Sens. Actuators **76**, 89–92 (1999).
[9]Y. Q. Fu, J. K. Luo, X. Du, A. J. Flewitt, Y. Li, A. Walton, and W. I. Milne, Sens. Actuators B **143**, 606–619 (2010).
[10]J. Friend and L. Y. Yeo, Rev. Mod. Phys. **83**(2), 647–704 (2011).
[11]R. Shilton, L. Y. Yeo, and J. R. Friend, Sens. Actuators B **160**(1), 1565–1572 (2011).
[12]C. J. Strobl, A. Rathgeber, A. Wixforth, C. Gauer, and J. Scriba, paper presented at the Ultrasonics Symposium, 2002. Proceedings. 2002 IEEE, 2002.
[13]A. Wixforth, C. Strobl, C. Gaue, A. Toegl, C. Scriba, and Z. V. Guttenberg, Anal. Bional. Chem. **379**, 982–991 (2004).
[14]A. Wixforth, Superlattices Microstruct. **33**, 389–396 (2003).
[15]R. Shilton, M. K. Tan, L. Y. Yeo, and J. R. Friend, J. Appl. Phys. **104**(1), 014910–014919 (2008).
[16]A. Rathgeber, M. Wassermeier, and A. Wixforth, J. ASTM Int. **2**(6), **259–266** (2005).
[17]K. Sritharan, C. J. Strobl, M. F. Schneider, A. Wixforth, and Z. Guttenberg, Appl. Phys. Lett. **88**(5), 054102–054103 (2006).
[18]W. Tseng, J. Lin, W. Sung, S. Chen, and G. Lee, J. Micromech. Microeng. **16**, 539–548 (2006).
[19]M. K. Tan, J. R. Friend, and L. Y. Yeo, Phys. Rev. Lett. **103**(2), 024501 (2009).
[20]M. K. Tan, L. L. Yeo, and J. R. Friend, paper presented at the IEEE International Ultrasonics Symposium (IUS, Rome, Italy), 2009.
[21]M. K. Tan, L. Y. Yeo, and J. R. Friend, EPL (Europhys. Lett.) **87**(4), 47003 (2009).
[22]M. K. Tan, L. Y. Yeo, and J. R. Friend, Appl. Phys. Lett. **97**(23), 234106 (2010).
[23]M. Maezawa, R. Kamada, T. Suda, and T. Kamakura, paper presented at the Proceedings of 20th International Congress on Acoustics, Sydney, Australia, 2010.
[24]M. Tan, J. Friend, and L. Yeo, paper presented at the Proc. 16th Australasian Fluid Mech Conf., Gold Coast, Australia, 2007.
[25]J. Berthier, *Microdrops and Digital Microfluidic* (William Andrew Inc., Norwich, USA, 2008).
[26]A. Gantner, R. H. W. Hoppe, D. Köster, K. Siebert, and A. Wixforth, Comput. Vis. Sci. **10**(3), 145–161 (2007).
[27]M. Alghane, B. X. Chen, Y. Q. Fu, Y. Li, J. K. Luo, and A. J. Walton, J. Micromech. Microeng. **21**, 015005 (2011).
[28]M. Alghane, Y. Q. Fu, B. X. Chen, Y. Li, M. P. Y. Desmulliez, and A. J. Walton, J. Appl. Phys. **109**, 114901 (2011).
[29]S. Shiokawa, Y. Matsui, and T. Ueda, paper presented at the Proceedings of IEEE Ultrasonics Symposium (Montreal, 1989).
[30]K. Chono, N. Shimizu, Y. Matsui, J. Kondoh, and S. Shiokawa, Jpn. J. Appl. Phys., Part 1 **43**, 2987–2991 (2004).
[31]S. V. Patankar, *Numerical Heat Transfer and Fluid Flow* (Hemisphere, New York, 1980).
[32]B. H. Weigl, R. L. Bardell, and C. R. Cabrera, Adv. Drug Delivery Rev. **55**(3), 349–377 (2003).
[33]X. Y. Du, M. E. Swanwick, Y. Q. Fu, J. K. Luo, A. J. Flewitt, D. S. Lee, S. Maeng, and W. I. Milne, J. Micromech. Microeng. **19**, 035016 (2009).
[34]C. K. Fredrickson and Z. H. Fan, Lab chip **4**(6), 526–533 (2004).
[35]S. K. R. S. Sankaranarayanan, S. Cular, V. R. Bhethanabotla, and B. Joseph, Phys. Rev. E **77**(6), 066308 (2008).
[36]T. A. Franke and A. Wixforth, Chem. Phys. Chem. **9**, 2140–2156 (2008).
[37]J. Lighthill, J. Sound Vib. **61**, 391–418 (1978).
[38]J. Kondoh, N. Shimizu, Y. Matsui, M. Sugimoto, and S. Shiokawa, paper presented at the IEEE Sensors, 2005.
[39]T.-D. Luong, V.-N. Phan, and N.-T. Nguyen, Microfluid. Nanofluid. **10**(3), 619–625 (2011).